



Investigation of Failure Behavior of a Thermoplastic Elastomer Gel

Journal:	<i>Soft Matter</i>
Manuscript ID	SM-ART-07-2018-001397.R1
Article Type:	Paper
Date Submitted by the Author:	08-Aug-2018
Complete List of Authors:	Mishra, Satish; Mississippi State University, Dave C. Swalm School of Chemical Engineering Maria Badani Prado, Rosa; Mississippi State University, Chemical Engineering Lacy, Thomas; Texas A&M University, Mechanical Engineering Kundu, Santanu; Mississippi State University, Chemical Engineering



Cite this: DOI: 10.1039/xxxxxxxxxx

Investigation of Failure Behavior of a Thermoplastic Elastomer Gel[†]

Satish Mishra,^a Rosa Maria Badani Prado,^a Thomas E. Lacy,^b and Santanu Kundu^{a*}

Received Date

Accepted Date

DOI: 10.1039/xxxxxxxxxx

www.rsc.org/journalname

Gels are increasingly being used in many applications, and it is important to understand how these gels fail due to mechanical deformation. Here, we investigate the failure behavior of a thermoplastic elastomer gel (TPEG) consisting of poly(styrene)-poly(isoprene)-poly(styrene) in mineral oil, in tensile mode, under constant stress, and in fracture tests, where the fracture initiates from a predefined crack. In these gels, the poly(styrene) endblocks associate to form spherical aggregates, as captured using SAXS. Shear-rheology experiments indicate that the poly(isoprene) midblocks connecting these aggregates are loosely entangled. The relaxation behavior of these gels has been captured by time-temperature superposition of frequency sweep data and stress-relaxation experiments. The relaxation process in these gels involves endblock pullout from the aggregates and subsequent relaxation of the chains. An unfavorable enthalpic interaction between the endblock and mineral oil results in a significantly large relaxation time. These gels display rate dependent mechanical properties, likely due to the midblock entanglements. Fracture and creep failure tests provide insights into the gel failure mechanism. Creep experiments indicate that these gels fail by a thermally activated process. Fracture experiments capture the energy release rate as a function of crack-tip velocity. The critical energy release rate is estimated by incorporating the friction force the polystyrene chains are subjected to as those are pulled out of aggregates, and the enthalpic cost to overcome unfavorable interaction between poly(styrene) and mineral oil. Our results provide further insights to the failure behavior of the self-assembled TPEGs.

1 Introduction

Thermoplastic elastomer gels (TPEGs) are a class of polymeric gels that behave like an elastic material at the application condition but soften and flow upon heating.^{1–14} TPEGs commonly

consist of a thermoplastic triblock copolymer [ABA] in a midblock (B) selective solvent. In these triblock copolymers, the endblocks (A) are glassy, and the midblocks are rubbery. In the gel state, the endblocks associate to form aggregates acting as crosslinks, whereas, the midblocks bridge those aggregates leading to a three-dimensional swollen, physically crosslinked network (or physical gels). The mechanical properties of these gels vary with the underlying structure, which depends on the polymer concentration, polymer architecture (molecular weight and block length), and polymer-solvent interaction. The interaction between the polymer and solvent is a strong function of temperature, rendering these gels thermoreversible. The endblock aggregates are typically spherical at lower polymer concentration,^{4,5,12,14} but can transform to cylinders or larger clusters with an increase in polymer concentration or decrease in tempera-

^a Dave C. Swalm School of Chemical Engineering, Mississippi State University, MS State, MS 39762. *E-mail: santanukundu@che.msstate.edu

^b Department of Mechanical Engineering, Texas A&M University, College Station, TX 77840.

[†] Electronic Supplementary Information (ESI) available: Temperature sweep experiment with $\gamma = 0.01$, and $\omega = 100$ rad/s, SAXS experimental data with model fit and schematic of gel structure, LAOS data at different polymer concentrations, stress versus initial sample stretch ratio for a MS fracture experiment, crack length versus time for a MS fracture experiment, crack length versus time for a QS fracture experiment, and force versus stretch ratio for a QS fracture experiment. See DOI: 10.1039/b000000x/

ture.^{14,15}

The TPEGs are highly stretchable and display significantly higher fracture toughness,^{5,16,17} that make them attractive for many applications, including ballistic applications,¹⁶ microfluidic devices,¹⁸ dielectric elastomers,¹⁹ and prosthetic and personal applications.²⁰ Since these TPEGs are subjected to mechanical deformation,^{16,21} it is extremely important to understand the failure behavior of these gels. But such understanding is lacking, despite significant insights in the gelation process and structure of these gels.^{2-6,9-11,14} Towards that goal, we investigate the failure behavior of a gel consisting of poly(styrene)-poly(isoprene)-poly(styrene) in mineral oil (referred to as SIS gel hereafter) subjected to tensile deformation, a constant load (creep failure), or fracture initiated from a defect.

In general, two different TPEGs have been commonly discussed in the literature: (i) poly(styrene)-rubber-poly(styrene), in the midblock selective solvents such as mineral oil, tetradecane, and squalane. The rubbery block can be poly(isoprene), poly(ethylene/butylene) or poly(ethylene/propylene). (ii) poly(methyl methacrylate)-poly(n-butylacrylate)-poly(methylmethacrylate) in 2-ethyl-1-hexanol or n-butanol (referred to as acrylic gel hereafter). Since mechanical characterization of soft gels using conventional tools is difficult, most of the literature data on these gels are based on conventional shear-rheology.^{2-6,9,10,12,14,16,22} Particularly, the shear-rheology experiments have been able to capture the relaxation behavior, which involves endblock pullout from aggregates and subsequent reattachment to another aggregate.^{4,10,12,13} The relaxation time has been shown to depend on the polymer block molecular weights,^{3,4,13} temperature,¹⁴ and the presence of nanoparticles.¹² It has been shown that in simple-shear mode, fracture takes place through strain localization, described as the damage accumulation in the deformed network, leading to localized failure of the gel.⁹ Fracture in physical hydrogels differs from that in the chemically crosslinked gels (or chemical gels), as the former involves breaking of physical bonds, or chain pullout from the aggregates, in comparison to the scission of chemical bonds in chemical gels. For [ABA] copolymer gels in a midblock selective solvent, there is an unfavorable enthalpic interaction between the endblocks and the solvent, which complicates the understanding of fracture process.^{7,8,13}

Because of their applications in many areas, tension, compression, creep, and fracture behavior of TPEGs are increasingly being studied using custom-developed tools/ techniques.^{5,16,17,23} In a recent study, rate-dependent mechanical properties of poly(styrene)-poly(ethylene/butylene)-poly(styrene) (or SEBS) gels have been captured.^{16,17} Failure behavior of acrylic gels has also been investigated using cavitation rheology experiments.^{11,24} Interestingly, the critical pressure for cavitation- the pressure at which a sudden expansion of cavity volume takes

place- has been found to be higher than that predicted by the Gent model, estimated through an analytical approach and finite-element modeling.^{11,24-28} Such behavior has been attributed to the fracture in the gels that takes place during the rapid cavity growth.¹¹ Failure of acrylic gels has also been investigated and it has been demonstrated that the energy release rate (Γ) -the energy required to create a unit surface area²⁹- increases with increasing polymer concentration and midblock molecular weight.⁵ Also, Γ displays a power law dependence with the crack-tip velocity. Such velocity dependence can be attributed to the viscous drag that those chains experience when stretched through the solvent (and any other viscous dissipation processes). At a sufficiently low crack-tip velocity, the viscous dissipation can be ignored and a critical or threshold energy release rate (Γ_0) can be obtained.^{23,30,31} In many gels, creep experiments, which are relevant to numerous applications, provide additional information regarding failure under constant stress with magnitude higher than the shear modulus. For biopolymer gels, creep experiments capture delayed fracture behavior.³²⁻³⁴ For polyampholyte hydrogels, Gong et al. reported a thermally activated process.³⁵ For TPEGs, creep failure has not been investigated widely, therefore motivating us to compare the behavior of these gels with other soft gels.

In addition, the experimentally determined value of Γ_0 needs to be compared with the theoretical prediction using scaling arguments to achieve further understanding of the gel failure process. For vulcanized rubbers and other chemically crosslinked networks without any solvent, the Lake and Thomas (LT) theory provides a good estimate of Γ_0 .³⁶ According to this theory, when a bond in a chain breaks during the fracture process, the energy stored in the chain is released.³⁶⁻³⁹ The LT theory has also been extended to chemical gels with some success, but this theory typically underpredicts Γ_0 , in comparison to the experimental results.^{23,30,31,39,40} The origin of such a discrepancy is still an open question.^{31,40} For the TPEGs, application of LT theory is not straightforward, as the fracture process involves chain pullout from aggregates and unfavorable interactions between the endblocks and the solvent.

To elucidate the failure behavior of TPEGs, we consider a physically assembled gel of SIS in mineral oil. Due to the long midblock length, the midblocks in these gels are expected to be entangled. Rheology experiments have been conducted to capture the relaxation mechanism and the level of entanglement. Small angle X-ray scattering experiments (SAXS) were used to investigate the gel microstructure. The failure behavior of these gels has been investigated through tensile, creep, and fracture experiments. Tensile experiments were carried out in order to demonstrate the strain rate dependence and entanglement effect on the mechanical properties. Further, the creep failure experiments provide information regarding the activated volume and bond lifetime.

At last, an attempt has been made to relate the experimentally determined energy release rate to the gel network structure.

2 Experiment Details

For the present study, we chose D1164 (provided by Kraton Inc.) as a polymer and Klearol[®] white mineral oil (provided by Sonneborn Inc.) as a midblock selective solvent. D1164 is an [ABA] triblock copolymer where the "A" block is poly(styrene) (PS) and the "B" block is poly(isoprene) (PI). The molecular weight of D1164 was measured using an Agilent GPC at 135 °C using 1,2,4-trichlorobenzene as solvent. Based on the polystyrene standards, the overall number average (M_n) and weight average (M_w) molecular weight of the polymer were determined as ≈ 112 kg/mol and ≈ 125 kg/mol, respectively. Based on the manufacturer datasheet, the average PS content of the polymer is 29 wt% and the PI content is 71 wt%. Since a polymer chain consist of two PS endblocks, molecular weight of each PS endblock is $M_{n,PS} \approx 0.29 \times 112 / 2 \approx 16.2$ kg/mol ($DP \approx 156$) and the molecular weight of midblock PI is $M_{n,PI} \approx 79.4$ kg/mol ($DP \approx 1166$). A TA Instruments Discovery HR-2 hybrid rheometer equipped with a Peltier plate was used for the rheological investigations. A 25 mm diameter parallel plate geometry with a gap of 1 mm was used for all experiments. To avoid the sample slippage at the rheometer plates, a 240 grit silicon carbide adhesive-backed sandpaper (Allied High Tech Products Inc.) was attached to the top and bottom plates.

For sample preparation, D1164 with specified proportion was dissolved in mineral oil at 140 °C for 6 h by using a magnetic stirrer (at 200 rpm). To remove any possible concentration gradient, the sample was further mixed using a vortex mixer at 1200 rpm for 30 s. The sample was then placed in an oven at 140 °C for 6 h to obtain a transparent solution without any bubbles. Most of the experiments conducted here have been performed on the 20% gel (w/w), which is equivalent to 18.1%(v/v) (volume fraction, $\phi = 0.181$) considering the specific gravity of polymer and the solvent as 0.94 and 0.83, respectively. To prepare the gel samples, the polymer solution was removed from the oven and was rapidly poured in a flat mold with a depth of 1 mm. The sample was then cooled at room temperature for 30 minutes to allow the gelation to take place. The gel sample was then cut into smaller pieces for rheology experiments. The rheometer bottom plate was heated to 100 °C for sample loading and was cooled down to the experimental temperature after sample loading. During cooling, a small amount of negative normal force developed, which was eliminated by compressing the sample further by about 30 μm before starting the experiments.

Small angle X-ray scattering (SAXS) results were obtained at room temperature using a SAXS setup at the University of Southern Mississippi with a 10 m beamline. A custom NCNR macro in Igor Pro (version 6.37) and a custom built script were used for

data fitting.^{14,44}

Tensile and creep failure experiments were performed at room temperature using a custom built setup shown in Figure 1A-B. Dogbone samples with gauge length, $l_{T0} = 4.2$ mm, breadth, $b_{T0} = 4.2$ mm, and thickness, $t_{T0} = 9.5$ mm (Figure 1A) were used.¹⁶ These dimensions were similar to that reported by Mrozek et al.¹⁶ As shown in Figure 1B, instead of using clamps, the dogbone sample was held by the help of four supporting pins fixed to the top and bottom supporting blocks. During an experiment, the sample was stretched by moving the top supporting block using a moving stage (M414, Physik Instrument) (Figure 1B). LabVIEW software (NI Instruments) was used for data capture and for controlling the experimental setup. A monochrome camera (Grasshopper3, Point Grey Research Inc.) was used to capture images at ≈ 18 fps during the experiments. The gel samples were marked with 3 lines, *viz.*, 1, 2, 3 (Figure 1A) in the gauge region. The distances between lines (*i.e.*, 1-2, 2-3, and 1-3) during sample stretching were estimated using a custom-built image analysis program developed in MATLAB with an accuracy of ≈ 0.08 mm. The stretched distance between two lines divided by their initial distance was used to estimate the stretch ratio (λ). This information was used to estimate a stretch rate ($\dot{\lambda} = d\lambda/dt$).¹⁶ Tensile tests were performed at three $\dot{\lambda} \approx 0.0048$, 0.048, and 0.455 s^{-1} , corresponding to the three moving-stage or stretch velocities of 0.1, 1, and 10 mm/s, respectively. The nominal (engineering) stress (σ_0) value was calculated based on the initial cross sectional area of the sample gauge region ($b_{T0} \times t_{T0}$). Experiments were repeated 8 times for each $\dot{\lambda}$. The Savitzky-Golay filter was used for data smoothing.

The creep failure experiments were performed for a set of σ_0 values. Here, the sample was stretched with a stretch velocity of 1 mm/s until a prescribed stress value was attained. Using a feedback loop in LabVIEW, a constant σ_0 value on the sample was maintained and the sample failure through crack initiation and propagation was monitored. The failure time was calculated from the time of application of full load to the time at which the fracture started. All experiments were repeated at least 20 times for each σ_0 value.

Fracture experiments were performed using a custom-built setup. A schematic of the setup is shown in Figure 1C. A mold was used to prepare the samples of length, $l_{F0} = 75$ mm, thickness, $t_{F0} = 4$ mm, and height, $h_{F0} = 50$ mm, respectively. The sample was gripped in-between two bars clamped together by using a Butterfly Wing hand screw-bolt. To avoid slippage at the grip, a soft textured shelf-liner (Duck Brand) was used. To facilitate the crack propagation, a notch with a dimension of $a_0 \approx 5$ mm was introduced at the middle of the sample using a sharp razor. The fracture experiments were performed in two different ways.²³ In the first set of experiments, the sample was stretched at 5 mm/s (stretch rate, $\dot{\lambda} = 0.1 \text{ s}^{-1}$) until the crack propagated

Table 1 Polymer Characteristics^{41–43}

Component	% wt	M_n (kg/mol)	M_e melt (kg/mol)	b (nm)	M_0 (kg/mol)	δ (M rad/s) ^{1/2}
PS	0.29	32.4	17	1.8	0.72	18.6
PI	0.71	79.4	6.4	0.84	0.120	16.6

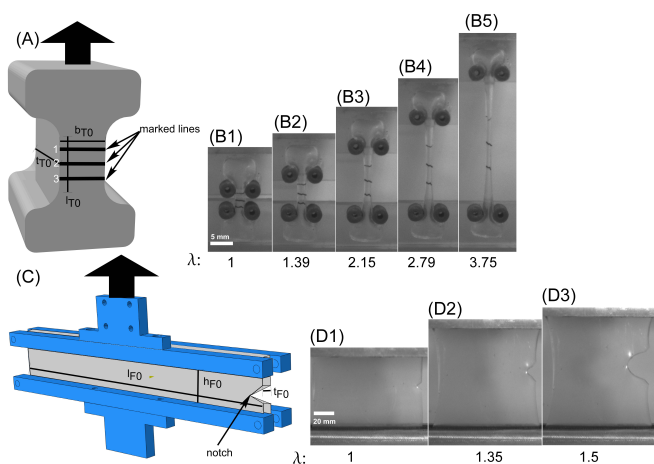


Fig. 1 (A) Schematic of a dogbone sample for the tensile and creep tests with the sample dimensions. Solid arrows represent the stretching directions. (B) Stretched sample at the stretch ratio (λ) of 1, 1.39, 2.15, 2.79, and 3.75 (B1–B5) for the strain rate of $\dot{\lambda} = 0.455 \text{ s}^{-1}$. (C) Schematic of the fracture experiment setup with the sample dimensions. (D) Images capturing crack propagation as a function of stretch (λ) of 1, 1.35, and 1.5 (D1–D3).

to about one-third of the sample length. The stretching was then stopped and the crack propagated spontaneously to the end of sample length (l_{F0}) with a constant velocity. This set of experiments is referred to as the quasistatic experiment (QS).²³ In the second set of experiments, the sample was constantly stretched with a stretch velocity of 0.01 s^{-1} until the crack reached to the end of the sample. This is referred to as the material saving experiment (MS), as defined by Baumberger and coworkers.²³ All fracture experiments were repeated at least three times. For all these experiments, special attention was paid to avoid any unwanted visible cracks and defects in the samples.

3 Results and Discussion

3.1 Rheology

The SIS gels are thermoreversible in nature and gelation was captured as a function of temperature using shear-rheology. Figure 2A displays the storage (G') and loss moduli (G'') as a function of temperature over the range of 12–100 °C for a gel with the polymer volume fraction, $\phi \approx 0.181$. In the temperature sweep experiments, an oscillatory shear strain, $\gamma = \gamma_0 \sin(\omega t)$ was ap-

plied. Here, γ_0 is the strain amplitude, and ω is the applied frequency. In our case, $\omega = 1 \text{ rad/s}$, strain amplitude, $\gamma_0 = 0.01$, and cooling rate of 2 °C/min were used. At $T > 85 \text{ °C}$, the G'' is higher than G' indicating a sol state. A crossover between G' and G'' is observed at $T \approx 85 \text{ °C}$, which is referred to as the gelation temperature, T_{gel} . Below T_{gel} , G' is greater than G'' and continues to increase until it reaches an apparent plateau below 42 °C . Such a plateau indicates that the gel structure does not undergo a significant change below that temperature. This is important as the tensile, creep, and fracture experiments were performed at room temperature ($\approx 22 \text{ °C}$). A knee in G' is observed at about $T \approx 75 \text{ °C}$. This knee is likely due to the result of an order-to-disorder transition (ODT).⁴⁵ The gelation temperature displays a frequency dependence, as increasing the frequency to 100 rad/s during the temperature sweep experiment shifts the gelation to a higher temperature. Because of a limitation in our rheometer, the shifted T_{gel} could not be determined precisely (phase angle became $> 90 \text{ °}$ for $T > 82 \text{ °C}$ at $\omega = 100 \text{ rad/s}$), but from the Figure S1 in the Supporting Information, the shifting T_{gel} to a higher temperature is evident.

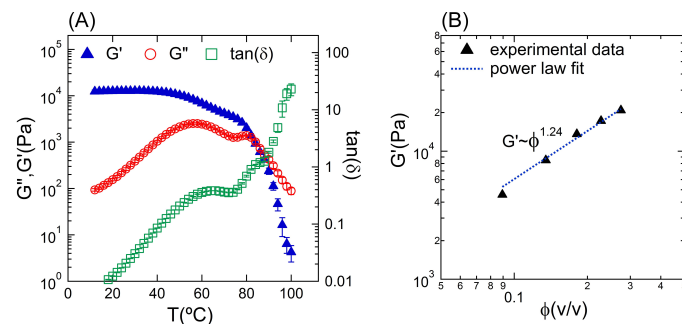


Fig. 2 Temperature and concentration dependence of SIS gels. (A) Evolution of G' , G'' , and $\tan(\delta)$ as a function of temperature for a gel with $\phi \approx 0.181$. (B) G' as a function of polymer volume fraction (ϕ). The symbols represent the experimental data and the dashed line represents the power law fit, $G' = C\phi^n$, where C is a constant. The error bars represent one standard deviation.

Gelation and microstructural development of [ABA] triblock copolymers in midblock selective solvents have been discussed in the literature extensively.^{2,7,8,11–13,15,46–48} Based on that understanding, we can infer that at high temperatures a viscous solution will be obtained as both PS and PI blocks are soluble in

mineral oil. The PS solubility decreases with decreasing temperature, however, the PI solubility does not change significantly. The Hansen solubility parameter (δ) of mineral oil $\approx 14.1 \text{ MPa}^{1/2}$ is closer to that of PI $\approx 16.6 \text{ MPa}^{1/2}$ (Table 1), which further supports that the mineral oil is a good solvent for the PI.^{2,43} With decreasing temperature, the PS endblocks collapse, and a majority of those collapsed endblocks associate to form aggregates. The PI midblocks form bridges between these aggregates. Such self-assembly results in a three-dimensional network formation. Figure S2B in Supporting Information represents a schematic of the possible gel structure. If the midblock is sufficiently long and the polymer concentration is low, both endblocks can remain in one aggregate, forming a loop.^{3,48} Experimental and simulation studies have captured the bridge versus loop formation in these gels.^{49,50} For the SIS gel in n-tetradecane, it has been shown through dielectric measurements that the bridging fraction (BF) is higher than the loop fraction, and the BF increases with polymer concentration.⁴⁹ DPD-mSRP simulations captured increasing BF with increasing midblock length, and for an entangled system, the BF saturates at ≈ 0.6 .⁵¹

G' values for different polymer volume fractions have been measured at 22 °C using $\gamma_0 = 0.1$ and $\omega = 100 \text{ rad/s}$ are shown in Figure 2B. At this frequency, G' is independent of frequency. For all polymer volume fractions investigated here, G' is an order of magnitude higher than G'' indicating the samples are in a gel state at room temperature (Figure S3). A power law fit captures the trend, $G' \sim \phi^{1.24}$ (Figure 2B). Since the exponent of 1.24 is less than the theoretical prediction of ≈ 2.3 for entangled systems,^{42,50,52} we can consider that the midblocks are loosely entangled in our gels. The entanglements present in this system are most likely trapped entanglements. It is unlikely that the chains would disentangle during the mechanical deformation, as that would involve chain pullout from the aggregates followed by disentanglement through the relaxation process. Note that the M_n of PI for the present system is greater than the entanglement molecular weight (M_e) of the melt (Table 1). However, in a good solvent, the number of PI entanglements (n_e) would be lower than that observed in melt. In the PI melt, the number of entanglements, $n_{e,\phi=1} = M_{n,PI}/M_{e,PI} \approx 12.4$, whereas, for $\phi = 0.181$, the volume fraction at which most of the experiments were conducted in this study, $n_{e,\phi=0.181} \approx n_{e,\phi=1}\phi^{4/3} = 1.3$.^{51,52} Such a small number of entanglements further supports the loosely entangled nature of our gel. As shown below, these entanglements also act as crosslinking points and increase the modulus of these gels during deformation.⁴² Note that power law exponents lower than 2.3 has also been reported in previous studies consist of entangled SIS gels, such as 2.15 (M_w of the polymer $\approx 133.3 \text{ kg/mol}$ with PS wt% ≈ 13.5)³ and 1.77 (M_n of polymer $\approx 260 \text{ kg/mol}$ with PS wt% ≈ 55).² However, gels of poly[styrene-co(ethylene/butylene)-styrene] (SEBS gel from here

Table 2 Fitted parameters from SAXS results

core radius, r_0 (nm)	hard sphere thickness, s (nm)	polydispersity, (σ/r_0)	volume fraction, (ψ)
8.21	8.82	0.09	0.42

after) in mineral oil, Laurer et al. reported an exponent of 2.68.²

The evolution of SIS gel microstructure with the change of styrene weight fraction in the gel (w_s) has been reported in the literature.² It has been shown that the spherical micellar morphology at low PS weight fraction ($w_s \leq 0.16$) evolved into cylindrical and then to a lamellar structure at high w_s .² In our system, w_s is ≈ 0.058 for $\phi = 0.181$, which is similar to the lowest w_s investigated by Laurer et al. ($w_s \approx 0.05$).² Therefore, a spherical micellar morphology is expected. Such morphology has also been observed for other triblocks gels such as acrylic gels,^{4,5,14} and SEBS gels.¹³

To characterize the network structure further, SAXS experiment was performed on a $\phi = 0.181$ gel at room temperature. The intensity profile (I) as a function of the scattering vector (q) is shown in the Supporting Information (Figure S2A). The intensity profile resembles that observed for acrylic gels,^{4,14} with a distinct peak at $q = 0.02 \text{ \AA}^{-1}$, representing a Bragg peak. The Gaussian polydispersed-core hard sphere model (Figure S2B) is fitted to the experimental data.^{4,14,53} Here, the core represents spherical aggregates with radius, r_0 . The core-radius follows a Gaussian distribution, with σ is the standard deviation and the polydispersity is σ/r_0 .^{14,53} The fictitious hard spheres have radius of $r_0 + s$, where s is the hard sphere thickness. Twice the fictitious hard sphere thickness ($2s$) is a measure of the inter-aggregate distance. As shown in Figure S2A, this model can capture the scattering data reasonably well and the fitted parameters are shown in Table 2. In addition to r_0 , s , and σ/r_0 , we have also determined the hard sphere volume fraction, ψ . Although, there is an evidence of ODT in rheological experiments, SAXS data does not manifest any ordered structure, such as BCC (body-centered cubic), as observed in many [ABA] gels.^{13,15} Such differences can be attributed to the different cooling cycles that the samples were subjected to during these experiments. This will be further investigated in a future study.

Large amplitude oscillatory shear (LAOS) experiments were performed at 22 °C and $\omega = 1 \text{ rad/s}$, where γ_0 was varied from 10^{-4} to a large strain of 1. The G' values are two order of magnitude higher than the G'' (Figure S3), thus, the gel is mostly elastic at room temperature. G' values do not change significantly over the strain values investigated here. The corresponding third order Chebyshev coefficients (e_3), which capture the non-linearity of a sample, are also very small.^{11,54} Therefore, the gel displays

linear-elastic behavior up to the γ_0 of 1 for the applied frequency (or strain-rate). Also, the samples do not undergo failure/fracture at the maximum strain range investigated here. At $\gamma_0 \geq 1$, the instrument's maximum torque limit was reached and γ_0 was not increased further.

Strain stiffening behavior has been reported for some physically assembled [ABA] gels in midblock selective solvents, for example, acrylic gels in 2-ethyl-1-hexanol and n-butanol. The responses have similarities to that observed in biopolymer gels, e.g., actin, collagen, and alginate gels.^{6,9,11,14,55} The strain-stiffening behavior of the [ABA] gels has been explained in terms of finite chain extensibility of the midblock. With applied strain, the midblock approaches its maximum extensibility before the end-blocks pull out of the aggregates. This results in strain-stiffening behavior. However, no negative normal stress, commonly observed in many strain-stiffening biological gels, has been observed for these self-assembled [ABA] gels.^{55,56} We have not observed strain-stiffening of the SIS gels over the strain range investigated here, though it may be possible that the strain-stiffening takes place at a higher strain. Due to the long midblock length, the applied strain needs to be very high to reach the maximum extensibility of the PI chains, which cannot be achieved in a shear-rheometer. Alternatively, non-linear rheological responses can be accessed at low strain but at very high strain rates,¹¹ however, this has not been attempted in this study.

To investigate the relaxation behavior of these gels, frequency sweep experiments were performed for $\omega = 1 - 100$ rad/s using $\gamma_0 = 0.1$ over the temperature range of 12 – 82 °C. G' , G'' , and $\tan(\delta)$ are plotted as a function of ω in Figure 3. As shown in Figure 3A, at $\omega = 100$ rad/s, G' values are similar for all temperatures. However, at low frequency, G' decreases with increasing temperature. For $T < 42$ °C, G' displays a weak frequency dependence. That behavior can be attributed to the polymer-solvent interaction, as away from the T_{gel} , the structure formation through phase separation is complete.

We performed time-temperature superposition (TTS) on the frequency-sweep data collected at multiple temperatures and the results are shown in Figure 3B. Here, G' , G'' , and $\tan(\delta)$ are plotted against the shifted frequency ($a_T \omega$). We conducted a horizontal shifting along the ω -axis using a shift factor, a_T , considering 22 °C as the reference temperature (T_{ref}). a_T has been fitted with the Arrhenius equation, $\ln(a_T) = (E_a/R)(1/T_{ref} - 1/T)$ (Figure 3B inset), where E_a is the activation energy, and R is the gas constant. The fitting estimates the activation energy, $E_a \approx 200$ kJ/mol. Note that this value is lower than that observed for acrylic gels (≈ 550 kJ/mol),⁴ but similar to that observed for SIS (≈ 210 kJ/mol) and SEPS (≈ 220 kJ/mol) gels in squalane.³ Such a low value of activation energy supports the weaker temperature dependence of moduli.

A clear crossover between G' and G'' was not observed, i.e.,

the gel does not show a terminal relaxation behavior, as observed for some SEPS and SIS gels, particularly for low polymer concentration and low polymer molecular weight.^{3,13} But our results are similar to SEPS gels with high polymer molecular weight.¹³ The apparent plateau in G' at low frequency can be attributed to the formation of three-dimensional ordered structured (such as BCC) or "highly congested disordered micellar structure", as proposed by Lodge and coworkers.¹³ However, the latter appears to be relevant for our system, as the scattering data do not provide clear evidence of an ordered structure. Since there is no crossover frequency, we consider the apparent maximum in $\tan(\delta)$ at $a_T \omega \approx 10^{-5}$ rad/s to estimate the relaxation time. Correspondingly, the relaxation time is, $\tau_{FS} = 1/a_T \omega \approx 10^5$ s = 27.8 h. An Arrhenius law fit of a_T (Figure 3B inset) also indicates the single dominant relaxation mechanism in this system.⁴¹

As the maximum in the $\tan(\delta)$ has not been determined unambiguously, which is used in determining the relaxation time, the relaxation behavior is further investigated through stress relaxation experiments performed at $T = 22, 52, 62,$ and 72 °C, respectively. A shear strain of $\gamma_0 = 0.01$ was applied and the sample was allowed to relax for 30 minutes. Results are shown in Figure 4, in which time-dependent shear moduli $G(t)$ are plotted as a function of time for different temperatures. Solid lines represent the fitted stretched exponential function represented as:^{10,12,22,57}

$$G(t) = G_0 \exp(-(t/\tau_{SR})^\beta) \quad (1)$$

where τ_{SR} is the relaxation time, and β captures the distribution in relaxation time. G_0 is the zero strain shear modulus obtained from the temperature sweep experiment performed at $\omega = 100$ rad/s and $\gamma_0 = 0.01$ (Figure S1). Eq 1 can fit the results for temperature ≤ 62 °C, however, a poor fitting is observed for 72 °C, which is near T_{gel} . Table 3 summarizes the fitted parameters obtained for different temperatures.

Table 3 Fitted parameters and constants used to fit the Eq 1 with the stress relaxation responses

Temperature (°C)	G_0 (kPa)	τ_{SR} (s)	β
22	14.36	54118 ± 4750	0.11 ± 0.001
52	14.95	11.4 ± 0.074	0.22 ± 0.0005
62	14.37	1.98 ± 0.023	0.24 ± 0.001
72	12.34	0.52 ± 0.006	0.24 ± 0.001

An estimated relaxation time of $\tau_{SR} = 54118$ s ≈ 15 h is obtained at 22 °C and the relaxation time decreases with increasing temperature. The $\beta = 1$ indicates a single relaxation time, and the material follows the Maxwell model.¹² Whereas, $\beta < 1$ indicates a distribution in the relaxation time attributed to the variation in the network structure. We obtain β in the range of 0.11 to 0.24.

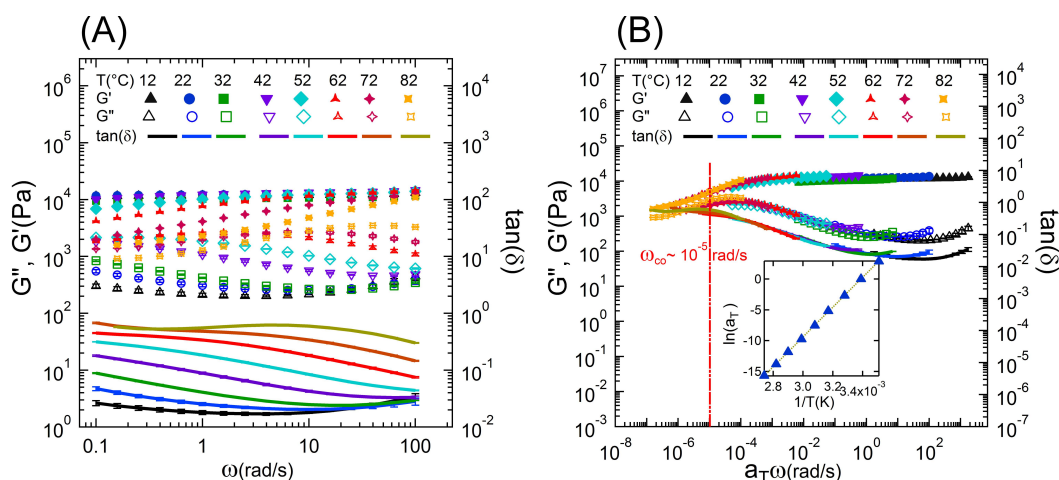


Fig. 3 Frequency sweep results for a gel with $\phi \approx 0.181$. (A) G' , G'' , and $\tan(\delta)$ are plotted as a function of ω for different temperatures. (B) Time-temperature superposition (TTS) of the frequency sweep data. The dashed line captures the maximum in the $\tan(\delta)$. Error bars represent one standard deviation. The inset graph shows the shift factor (a_T) as a function of temperature. Dotted line indicates the Arrhenius model fit.

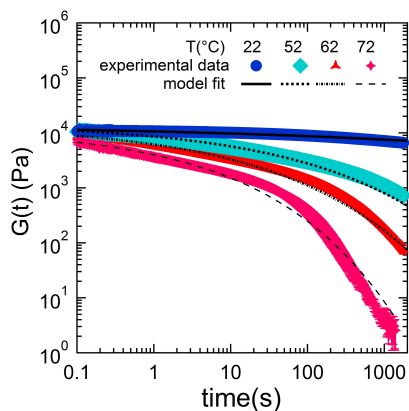


Fig. 4 Stress relaxation behavior at 22, 52, 62, and 72 °C, respectively. The solid markers represent the experimental data, whereas the lines represent fitting of the stretched exponential function (Eq 1).

Also, β is not constant over the temperature range investigated here, as reported for acrylic gel.¹⁰ However, we reported a non-constant β for acrylic gels with and without graphene.¹² Also, β in our case is smaller than that has been reported for acrylic gels,^{10,12,47} but similar to that observed by Hotta et al. for an SIS triblock copolymer, which was not a gel though.⁴¹ τ_{FS} and τ_{SR} are of the same order of magnitude. Therefore, we can consider that the relaxation time of our system as τ_{SR} , which has been determined without any ambiguity.

The relaxation process in our gel is associated with the end-block pullout from the aggregates followed by the relaxation of entangled midblocks.^{3,13} We can also estimate the Rouse re-

laxation time for the PS chains ($\tau_{Rouse,PS}$) to evaluate whether the relaxation process in our gel is being dominated by the relaxation of PS chains in the aggregates. Now, $\tau_{Rouse,PS} = \zeta b_{PS}^2 N_{PS}^2 / 6\pi^2 k_B T$.^{13,42} Here, ζ is the monomeric friction force, b_{PS} is the PS Kuhn length, N_{PS} is the number of Kuhn segments in a PS endblock (≈ 23), and k_B is the Boltzmann constant. The lowest temperature at which the ζ value reported is 100 °C, the glass transition temperature of PS.^{13,58} Considering the reported value of $\zeta \approx 1.2 \times 10^{-3}$ Ns/m at that temperature,^{13,58} we estimate $\tau_{Rouse,PS} \approx 8.54$ s, which is approximately four order of magnitude higher than τ_{SR} and τ_{FS} at 22 °C. No information regarding the solvation state of the PS aggregates in our gel is available, however, DSC data for acrylic gels captures a significant reduction of the glass transition temperature of the PMMA aggregates in comparison to that of the homopolymers.¹⁴ Also, for diblock poly(styrene)-poly(isoprene) polymers in tetradecane at low styrene concentration, the glass transition temperature of the styrene approaches 40 °C. For our analysis, we consider that the PS aggregates with some level of solvation are near their glass transition temperature. Both ζ and $\tau_{Rouse,PS}$ can be different than that considered here, but they are not expected to deviate significantly from the case considered here.

We can also determine the τ_{Rouse} of the PI chains as $\tau_{Rouse,PI} \approx \eta_s b_{PI}^3 N_{PI,e}^2 / k_B T$,⁴² where, b_{PI} is the PI Kuhn length, η_s is the solvent viscosity, and $N_{PI,e}$ is the number of PI Kuhn segments (≈ 662). We estimated $\tau_{Rouse,PI} \approx 4.53 \times 10^{-4}$ s, which is significantly lower than the measured relaxation time. Since fractional entanglement per chain, i.e., $n_e = 1.3$ estimated earlier is difficult to apprehend physically, we have approximated $n_e = 2$. Considering that we obtain, $\tau_{Rouse,PI} \approx 5.03 \times 10^{-5}$ s. Thus, the relaxation

observed in the gel is not an internal relaxation of PS within the aggregates or PI chain relaxation but a time scale related to the endblock pullout, $\tau_{pullout}$. Chain pullout kinetics for the dilute micellar solutions of diblock and triblock copolymers have been investigated using time-resolved small angle neutron scattering (TR-SANS), and the corresponding relaxation time has been related to that obtained from shear-rheology.^{7,8,13} Various other relaxation modes, including, "corona screening",⁵⁹ "double activation",^{60,61} and "walking diffusion"^{60,61} processes, have also been considered.

The relaxation time for chain pullout ($\tau_{pullout}$), which is $\sim \tau_{FS}$ or τ_{SR} , can be given as $\tau_{pullout} \approx \tau_{Rouse} e^{\alpha\chi N_{PS}}$.¹³ Here, χ is Flory-Huggin's parameter, and prefactor, α , is a fitted parameter obtained from TR-SANS experiments.^{7,8,13} $\alpha\chi N_{PS}$ represents an energy barrier associated with enthalpic unfavorable PS-mineral oil interactions (the solubility of PS endblocks in mineral oil is low at low temperature).¹³ Using the above relationship of $\tau_{pullout}$, and assuming that $\tau_{pullout}/\tau_{Rouse,PS} \approx 6.3 \times 10^3$, we can estimate $\alpha\chi \approx 0.38$, since α and χ values are not available for our case. With increasing temperature, PS solubility increases in the mineral oil. The endblock pullouts become easier and the crosslinks (aggregates) can become weaker, resulting in shorter relaxation times (see Table 3). Thus, polymer chain length, and solvent quality (therefore, temperature) dictate the relaxation time in these gels. In addition, loops will also attribute to the relaxation behavior. However, based on the computation studies the bridge fraction is expected to be higher than the loop fraction,⁵⁰ and in this study we have not made an attempt to measure that experimentally.

3.2 Failure in Tensile Mode: Effect of Strain Rate

Nominal stress (σ_0) versus stretch ratio (λ), obtained from the tensile tests conducted using a custom-built setup (Figure 1), are shown in Figure 5A. Three different $\dot{\lambda}$ s, spanning over three orders of magnitude have been considered. σ_0 is calculated by taking an average of eight runs, and the results are shown for the minimum failure stretch ratio out of these runs. Sample images during a typical tensile test for different values of λ and for $\dot{\lambda} = 0.455 \text{ s}^{-1}$ are shown in Figure 1B. Relatively high stretch ratio, $\lambda = 3.75$, emphasizes the high stretchability of this sample before failure.

At small λ , the results for three different $\dot{\lambda}$ overlap, indicating that at low strain the modulus is independent of strain-rate. However, at higher λ , the responses diverge and the modulus increases with increasing $\dot{\lambda}$. The observed increase in modulus can be attributed to the presence of entanglements in the system. These entanglements act as crosslinks and restrict the local movement of the midblock chains during the stretch.⁵⁰ Thus, entanglements increase the modulus and show a rate dependence behavior. For the entangled systems, a Slip Tube model estimates the nominal

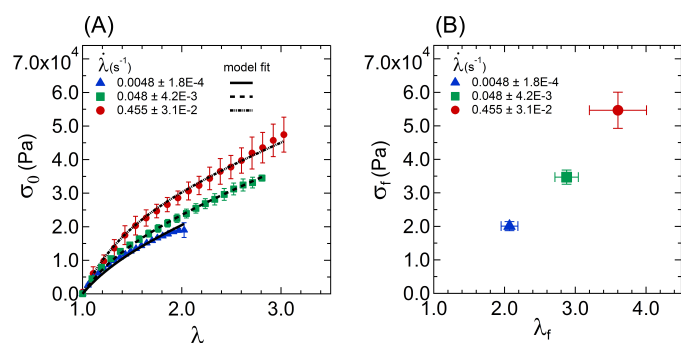


Fig. 5 Tensile test results at different $\dot{\lambda}$. (A) Nominal stress (σ_0) versus stretch ratio (λ) for $\dot{\lambda} = 0.0048, 0.048, \text{ and } 0.455 \text{ s}^{-1}$. The symbols represent the experimental data, whereas the lines are model fit with Eq 2. (B) Failure stress (σ_f) and failure stretch ratio (λ_f) for three $\dot{\lambda}$. Error bars represent one standard deviation.

elongation stress as:^{16,42,50,62}

$$\sigma_0 = \left(G_c + \frac{G_e}{0.74\lambda + 0.16\lambda^{-1/2} - 0.35} \right) \left(\lambda - \frac{1}{\lambda^2} \right) \quad (2)$$

Here, G_c is the modulus due to crosslinks, and G_e is the entanglement contribution to the elastic modulus. Fitting both G_c and G_e to the experimental data can potentially overpredict G_c .⁵⁰ Therefore, we fix G_c to be equal to $G' = 11.659 \text{ kPa}$. This is obtained from the TTS of frequency sweep experiments and corresponds to the G' value at $\omega = 10^{-3} \text{ rad/s}$ (Figure 3B), the lowest frequency at which the plateau in G' is observed. A plateau in frequency sweep indicates the response from the polymer network,^{13,63} and we can assume that at this frequency the effect of entanglement is not significant. The fitting provides $G_e = 0.082, 2.8, \text{ and } 8.8 \text{ kPa}$ for $\dot{\lambda} = 0.0048, 0.048, 0.45 \text{ s}^{-1}$, respectively. Thus, the effect of entanglement on our samples is evident from the tensile tests. In absence of entanglement, σ_0 is not expected to show $\dot{\lambda}$ dependence. This strain rate dependence captures the increase in entanglement contribution with increasing strain-rate.

Figure 5B displays nominal fracture stress (σ_f) and fracture strain (λ_f) for three different strain-rates. Both of these increase with increasing $\dot{\lambda}$. Previously, SEBS gels have been investigated using tensile tests and our results are similar to that study, particularly, the increase of modulus, σ_f , and λ_f with increasing $\dot{\lambda}$.^{16,17} Failure of these gels takes place through the endblock pullout from the aggregates. At higher $\dot{\lambda}$, the PI chains are stretched rapidly, and it is likely that the load is not transferred for chain pullout to take place. As a result, the PI chains can be stretched to a large ratio. Also, higher λ_f leads to a higher σ_f . In the above formulation (Eq 2), the effect of viscous dissipation has not been considered, as reported from compression testing of SIS gels.⁶⁴ In our sample, the G' is two orders of magnitude higher than the G'' and the viscous effect is likely to be insignificant.

3.3 Creep Experiments: Failure under Constant Stress

The results of the creep tests are shown in Figure 6. We have considered five constant nominal stress values of 15, 17.5, 20, 22.5, and 25 kPa, respectively. These nominal stress values (σ_0) were 1.28, 1.50, 1.71, 1.93, and 2.14 times the G' value of 11.659 kPa, respectively. For each σ_0 , twenty runs were conducted. Failure of the gel was not instantaneous and it takes some finite time before failure took place. Such behavior in gels has been discussed as a delayed fracture in literature.^{32–35,65,66} The failure times were not constant and a distribution in failure time was observed. Figure 6A shows fraction of failure events plotted as a function of failure time for $\sigma_0 = 25$ kPa. The Figure 6A clearly captures the stochastic nature of the failure. Figure 6B shows the arithmetic mean of the failure time (t_{break}) plotted against σ_0 .

Previously, delayed fracture in soft and heterogeneous materials has been explained in terms of crack nucleation theory.^{32,33,67,68} The waiting time (or delay time) has been attributed to the time required for a micro-crack to achieve the necessary energy to propagate.⁶⁹ Considering Pomeau theory of crack nucleation, $\ln(t_{break})$ is proportional to σ_0^{-4} .^{32,67,70} However, this scaling relationship cannot capture our experimental data, as shown in inset Figure 6B. Hence, the fracture in creep mode is not due to crack nucleation. The data indicates that the relationship between t_{break} and σ_0 is exponential. Therefore, we investigated the activated bond rupture theory (kinetic theory) to explain the creep failure behavior.⁶⁹

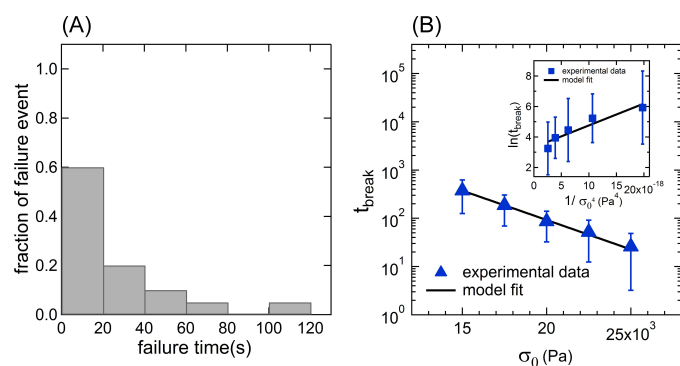


Fig. 6 (A) The distribution of failure event for $\sigma_0=25$ kPa. (B) Mean failure time (t_m) versus applied nominal stress (σ_0). The error bars represent one standard deviation. The line shows the model fit (Eq 3). The inset represents the fitting of $\ln(t_m)$ with σ^{-4} based on the Pomeau theory.³²

In order for chain pullout from the aggregate to lead to creep failure, the energy stored in the chain has to overcome the activation barrier, U_{act} . In absence of any load, the chain may acquire sufficient energy to overcome U_{act} due to thermal fluctuations. However, application of a load stretching the chain reduces the net energy required to overcome the activation barrier

by $U_{act} - \sigma_0 V$, where σ_0 is the applied stress and V is activation volume. If no load is applied, the endblock can attach to another aggregate (reassociation). If the chain-pullout and reassociation are in equilibrium, no fracture takes place. However, with the application of a load, the pullout events will be higher than the reassociation events. For this thermally activated process, the failure time can be expressed as:^{34,35,69,71}

$$t_{break} = t_0 \exp\left(\frac{U_{act} - \sigma_0 V}{k_B T}\right) \quad (3)$$

where, t_0 is the characteristic time related to the motion of PS chains. As indicated above, the numerator in exponent represents the net energy associated with chain pullout. The denominator represents the thermal energy corresponding to temperature T . As presented in Figure 6B, the Eq 3 fits the experimental data reasonably well. From fitting we obtain, $V \approx 1142$ nm³, which is about half of the volume occupied by an aggregate, $\frac{4}{3}\pi r_0^3 \approx 2318$ nm³. Interestingly, this is equivalent to the Eyring's theory, which predicts that the activation volume is half of the average volume occupied by a molecule.³⁴ Therefore, the aggregates are thermally activated during the process.³⁴

The extrapolation of the fitted line in Figure 6B to the zero stress gives $(t_{break})_{\sigma_0=0} \approx 19149$ s = 5.3 h, which can be understood as the strongest bond lifetime. This can be compared to the relaxation time estimated from the frequency sweep experiments $\tau_{FS} = 27.8$ h and the stress relaxation experiments $\tau_{SR} = 15.03$ h. All these values are not significantly different. However, it is important to note that for many systems, at low applied stress, the time to failure (t_{break}) increases significantly.³⁵

3.4 Fracture of Gels from a Pre-Defined Crack

Figure 7A represents the force (F) versus λ obtained from a typical material saving (MS) experiment. During initial stretching the crack length remained unchanged. This is evident from the Figure 7A inset, in which the crack length (a) did not change for $\lambda \leq 1.21$. During this process, the sample stored potential energy (ignoring any dissipation). This region can also be used to estimate modulus of the gel. Applying the neo-Hookean model at low strain, nominal stress, σ_0 can be related to λ as $\sigma_0 = (E/3)(\lambda - 1/\lambda^2)$, where E is the tensile modulus ($E \approx 3G'$ for an incompressible material).⁶² As shown in Figure S4, the fitting provides $G' = 10.9$ kPa ($\approx E/3$), similar to that observed in rheological experiments.

When the energy stored in the system becomes higher than the fracture energy of the gel, the crack length starts to increase. Since the sample is stretched continuously, the crack tip velocity increases with crack propagation. This can be inferred from an increasing slope of the a versus λ curve for $1.21 \leq \lambda \leq 1.51$ (Figure 7A inset). At a certain point ($\lambda \approx 1.51$), the net energy stored in the system becomes sufficient for the crack to propagate unstably

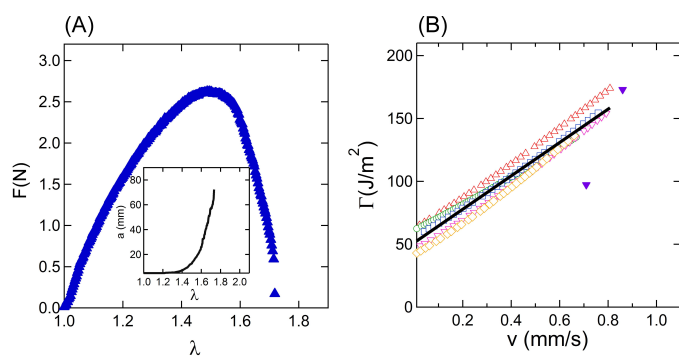


Fig. 7 Results from fracture test experiments. (A) Force (F) versus stretch ratio (λ) for a typical material saving (MS) experiment. Inset represents the crack length (a) as a function of λ . (B) The open symbols represent the energy release rate (Γ) versus crack tip velocity (v) obtained from the various MS experiments. The solid line represents the best fitting with Eq 5. Closed symbols represent results from QS experiments.

resulting in decrease in a recorded force. As shown in Figure 7A, consequently, a maximum in force response is observed at $\lambda = 1.51$.

From these results, energy release rate (Γ) can be estimated from the F versus λ results as:^{5,23}

$$\Gamma_i = \frac{h_{f0}}{t_{f0}l_{f0}} \int_{a_i}^{a_{i+1}} F_i d\lambda \quad (4)$$

where, F_i is the force applied to increase the crack length from a_i to a_{i+1} , while stretching the sample by $d\lambda$. For $1.21 \leq \lambda \leq 1.51$, a second order polynomial is fitted to the a versus time curve (Figure S5). The crack tip velocity (v) at a particular λ has been estimated by differentiating the fitted polynomial (Figure S5). Figure 7B displays the Γ versus v , where a linear increase in Γ with increasing v has been observed.

As described in the experimental section, a limited number of experiments were conducted, where a constant v was achieved (QS experiments). The constant velocity obtained in QS experiment is indicated in Figure S6. The Γ values from those experiments are also shown in Figure 7B. The corresponding F versus λ data are shown in Figure S7. Both MS and QS experiments, provided similar results, supporting the validity of the MS experiments.

The Γ versus v data is fitted with the following empirical model:^{72,73}

$$\Gamma = \Gamma_0 \left(1 + \left(\frac{v}{v^*} \right)^n \right) \quad (5)$$

Here, Γ_0 is the threshold energy release rate or critical energy release rate, v^* is the characteristic crack tip velocity, and n is an adjustable parameter that determines the shape of the curve. This equation has been traditionally used in contact mechanics to capture the crack propagation in pressure sensitive adhesives

(PSAs) and takes into account the viscoelastic response of the adhesive.^{72,73} Higher crack tip velocity leads to higher energy release rate because of the viscoelastic effect. In PSAs, the crack propagation takes place through the breaking of physical bonds, very similar to our case where cracks propagate by chain pullout (analogous to physical bond breaking). The increase of Γ with crack tip velocity in our gel can be attributed to the viscoelasticity, as described below.⁷⁴

Fitting Eq 5 to the experimental data provides, $\Gamma_0 \approx 51.25 \text{ J/m}^2$, and $1/v^* \approx 132.68 \pm 2.33 \text{ (mm/s)}^{-1}$ estimates $v^* \approx 3.86 \times 10^{-4} \text{ m/s}$, and $n = 1$.⁷² Γ_0 obtained for our sample is comparable to $\approx 10\text{-}20 \text{ J/m}^2$ obtained for a physically assembled acrylic gels. For these gels, it has been shown that Γ_0 depends on the endblock and midblock molecular weight, and the polymer concentration.⁵ For other physical gels, such as gelatin and alginate gels, Γ_0 was in the range of $1\text{-}5 \text{ J/m}^2$. For chemically crosslinked gels, such as polyacrylamide gels, Γ_0 can be of the order of 10 J/m^2 .³⁰ Γ_0 can be as high as $\approx 10^3 - 10^4 \text{ J/m}^2$, for strong, double network hydrogels.^{35,75,76}

The exponent, $n = 1$ obtained here from fitting Eq 5 warrants further discussion. This is different than $n = 0.4$ reported for acrylic gels.⁵ Also, for PSAs, typically $n = 0.6$ is reported.⁷² For gels, the variation in Γ with respect to the crack velocity can be explained in terms of the viscous contribution, which arises from the motion of PI chains relative to the solvent. It has been shown that for gelatin gels, such arguments lead to a linear velocity dependence, i.e., $\Gamma = \Gamma_0 + A\eta_s v$, where A is a constant.²³ Similar linear dependence has been observed for polyacrylamide gels in the fast crack-tip velocity region.³⁰ However for alginate gels, the linear dependence changes slightly if the zipping and unzipping events of ionic bonds are considered.³¹ Although the functional form used here is different, the similar linear dependency is most likely due to the effect of viscous drag on the PI chain movement.

The Γ_0 obtained here from fitting can be investigated further. Several attempts have been made in literature to estimate Γ_0 from classical LT theory, which was developed for chemically crosslinked rubber networks (without solvent).³⁶ According to this theory, $\Gamma_0 \sim NU\Sigma_{chain}$. Here, N is the degree of polymerization of the chains connecting two crosslinks, U is the bond energy (often C-C bond energy), and Σ_{chain} is the areal chain density. This theory indicates that before fracture the chain is fully stretched and the maximum energy that can be stored during that process is $\sim NU$. In chemically crosslinked samples, fracture takes place through bond breaking, and breaking of one bond results in the release of the energy stored in the chain. For physical gels considered here, fracture is not through bond-breaking but through chain pullout. Here, the energy stored per chain needs to be higher than the energy necessary for endblock pullout from an aggregate.

Since our midblock is entangled, it is expected that the strand

between the entanglement will be fully stretched. We can estimate the mean-square end-to-end distance of that strand as $\langle R_e^2 \rangle \approx N_{PI,e} b_{PI}^2$.⁴² Considering $n_e \sim 2$, we estimate $\langle R_e \rangle \approx 12.49$ nm and the fully-stretched length of the strand between the entanglement point is ≈ 185.6 nm. Therefore, the maximum stretch ratio will be $\lambda_{max} \approx 14.9$. Note that, in tensile testing we have not been able to achieve such high λ because of sample failure. In fracture experiments, as shown in Figure 1D, the crack front is highly stretched, but we have not attempted to estimate chain stretching. Without considering any enthalpic contribution, the free energy necessary to stretch the strand to the maximum extensibility is $\Delta F_{entropy} = k_B T (\lambda^2 + 2/\lambda - 3) / 2 = 4.4 \times 10^{-19}$ J $\approx 109 k_B T$.⁴²

We can then estimate the theoretical energy release rate, $\Gamma_{0,theo} \sim \Delta F_{entropy} \Sigma_{chain}$. Now, $\Sigma_{chain} = 1/(2s)^2 \approx 3.21 \times 10^{15}$ /m² and correspondingly, $\Gamma_{0,theo} \approx 1.43 \times 10^{-3}$ J/m², which is four orders of magnitude lower than the Γ_0 obtained by fitting Eq. 5 to our data. Note that instead of stretching of a strand between the entanglement, if stretching of the whole chain is considered (no entanglement), using a similar framework, we obtain $\Gamma_{0,theo} \approx 4.3 \times 10^{-3}$ J/m². The estimated value is still lower than that obtained experimentally. Therefore, the enthalpic contribution particularly that is associated with endblock-solvent interaction, and the friction the PS chains are subjected to with other PS blocks during pullout cannot be ignored.

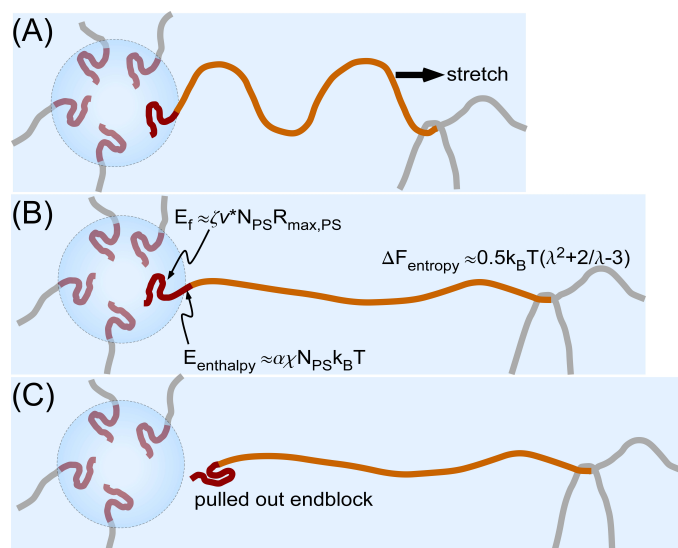


Fig. 8 A proposed mechanism for the chain pullout from the PS aggregates. (A) At equilibrium state, the end-to-end distance of a PI strand in between the aggregate and the entanglement is R_e . (B) The PI strand is stretched to its maximum contour length. The energy required to pullout from the chain consists of $E_{total} = \Delta F_{entropy} + E_f + E_{enthalpy}$. (C) Pullout of the endblock from the aggregate leading to the release of the stored energy.

Considering, the force (f) required to pull a chain out of the aggregate is $f \sim \mu_{mono} N_{PS}$, where μ_{mono} is the static monomeric friction coefficient per monomer.³⁷ From scaling arguments, the energy necessary for chain pullout is $E_f \sim f R_{max,PS}$, where $R_{max,PS}$ is the full chain length of PS ≈ 41.4 nm. μ_{mono} for polystyrene chains near glass transition temperature is not readily available in literature, but it can be estimated using the monomeric friction coefficient of polystyrene, $\zeta \approx 1.2 \times 10^{-3}$ Ns/m, as discussed earlier.^{13,58,77} From the monomeric friction coefficient and the characteristic crack tip velocity (v^*), we can approximate $\mu_{mono} \sim \zeta v^* = 4.64 \times 10^{-7}$ N/monomer, and the corresponding f is 1.1×10^{-5} N, which is much higher than the C-C bond scission force $\sim 2.2 \times 10^{-9}$ N, and therefore not realistic for physical gels.³⁷

Previously, an attempt has been made to estimate the force (f) necessary to pullout a chain from collapsed polystyrene micelles of diblock (SI) and triblock (ISI) polymers in n-hexane, a solvent for the PI block.⁷⁸ f has been determined to be in the range of $10^{-14} - 10^{-13}$ N, which depends on the block length, entanglements, and solvent quality. Since n-hexane ($\delta \approx 14.9$ MPa^{1/2}) is a relatively good solvent compared to mineral oil ($\delta \approx 14.1$ MPa^{1/2}) for PS, and the polymer concentration, particularly that of PI, is significantly higher in the present system, we expect a higher f . Considering, f of the order of 10^{-9} N, near the C-C bond energy, we estimate E_f equals to 4.14×10^{-17} J. This is the upper limit f and a reasonable approximation, as the PS aggregates are in the glassy state.

Since the endblock needs to overcome the unfavorable solvent interaction, the corresponding energy is $E_{enthalpy} \sim \alpha \chi N_{PS} k_B T \approx 3.57 \times 10^{-20}$ J. Therefore, the total energy necessary to pull a chain out of an aggregate is $E_{total} = \Delta F_{entropy} + E_f + E_{enthalpy} \approx 4.19 \times 10^{-17}$ J ($\Delta F_{entropy} = 4.43 \times 10^{-19}$ J, $E_f = 4.14 \times 10^{-17}$ J, $E_{enthalpy} = 3.57 \times 10^{-20}$ J). A schematic of the chain pullout is represented in the Figure 8. Using the Σ_{chain} estimated earlier, we obtain $\Gamma_0 \approx 0.135$ J/m², which is lower than that estimated by fitting Eq 5. Such a difference in comparison to the experimental data may result from endblock reassociation with another aggregate. Also, near the crack front solvent may diffuse from the highly stressed region to the bulk leading to increasing polymer concentration at the crack front. Both of these phenomena will likely cause a toughening effect in the gel, similar to that discussed for alginate gels.³¹ Also, from our analysis, it appears like frictional force experienced by the endblocks dictates the critical energy release rate. This will be further analyzed in the future, where the PS length will be maintained constant, but the mid-block length and the polymer volume will be varied.

Further, the sum of $E_f (\approx 1.02 \times 10^4 k_B T)$ and $E_{enthalpy} (\approx 8.76 k_B T)$ estimated here can be used as a measure of U_{act} in the Eq 3, as we could not determine the U_{act} from the creep data. Substituting $E_f + E_{enthalpy} \sim U_{act}$ in Eq 3 suggests the bond failure

time (t_{break}) at zero stress to be very high for any finite t_0 value. As indicated earlier, very high failure time at zero stress signifies that the thermal fluctuations may not be enough for sample failure. Although this has been predicted through a simulation study for a telechelic system,⁶⁹ further experimental investigation is needed.

3.5 Conclusions

SIS gel in mineral oil with polymer volume fraction, $\phi \approx 0.181$, exhibits micellar microstructure, in which the PS endblocks form aggregates. The aggregates are bridged by the PI midblocks forming a three-dimensional network. The midblocks are entangled because of the long midblock length, however, the shear-rheology data indicates that the entanglements are weak. Interestingly, these loosely entangled gels display rate-dependent tensile moduli and fracture strain. Relaxation processes in this gel depend on the endblock pullout of the aggregates. The gel relaxation time has been determined by stress-relaxation and frequency sweep experiments, and both of these experiments provide not a significant different results. The high relaxation time ($\approx 5.4 \times 10^4$ s), in comparison to the Rouse relaxation time of PS in the aggregates (8.53 s), has been attributed to the enthalpically unfavorable endblocks pullout in the solvent. Creep failure processes have been determined to be thermally activated, and the activation volume has been estimated to be one half of the crosslink size. This gel also exhibits significant toughness as the energy release rate was as high as 200 J/m^2 over the experimental conditions considered here. The energy release rate scales linearly with the crack-tip velocity. The critical energy release rate for this gel has been determined to be 51.25 J/m^2 . The experimentally determined value is compared with the value obtained theoretically by considering the frictional force necessary for chain pullout from the aggregates and enthalpic cost associated with endblock and solvent interaction. In summary, we characterize the failure behavior of a SIS gel in various modes of deformation. The fundamental understanding of the underlying mechanisms involved in the chain pullout has been presented. We have attempted to link the theoretically estimated and experimentally observed energy release rate. The results presented here are important for determining the application window for these thermoreversible, self-assembled block copolymer gels.

4 Acknowledgement

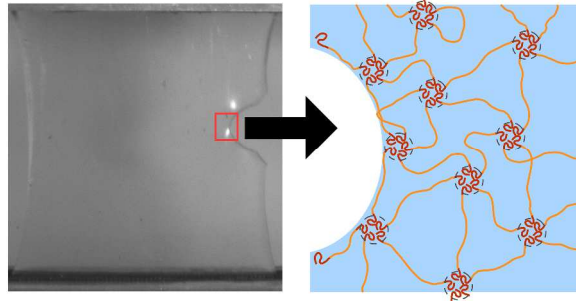
Authors acknowledge financial support from the National Science Foundation [DMR-1352572]. Authors are grateful to the Dr. Xiaodan Gu at the University of Southern Mississippi for conducting SAXS experiments, and Dr. Jason D. Azoulay at the University of Southern Mississippi for conducting GPC experiments. Authors are thankful to Dr. Dong Meng and Dr. Neeraj Rai at Mississippi State University for the helpful discussions.

References

- 1 C. L. Mowery, A. J. Crosby, D. Ahn and K. R. Shull, *Langmuir*, 1997, **13**, 6101–6107.
- 2 J. H. Laurer, S. A. Khan, R. J. Spontak, M. M. Satkowski, J. T. Grothaus, S. D. Smith and J. S. Lin, *Langmuir*, 1999, **15**, 7947–7955.
- 3 D. A. Vega, J. M. Sebastian, Y. L. Loo and R. A. Register, *J. Polym. Sci. Part B Polym. Phys.*, 2001, **39**, 2183–2197.
- 4 M. E. Seitz, W. R. Burghardt, K. T. Faber and K. R. Shull, *Macromolecules*, 2007, **40**, 1218–1226.
- 5 M. E. Seitz, D. Martina, T. Baumberger, V. R. Krishnan, C. Y. Hui and K. R. Shull, *Soft Matter*, 2009, **5**, 447–456.
- 6 K. A. Erk, K. J. Henderson and K. R. Shull, *Biomacromolecules*, 2010, **11**, 1358–1363.
- 7 S. H. Choi, T. P. Lodge and F. S. Bates, *Phys. Rev. Lett.*, 2010, **104**, 1–4.
- 8 S. H. Choi, F. S. Bates and T. P. Lodge, *Macromolecules*, 2011, **44**, 3594–3604.
- 9 K. A. Erk, J. D. Martin, Y. T. Hu and K. R. Shull, *Langmuir*, 2012, **28**, 4472–4478.
- 10 K. A. Erk and J. F. Douglas, *MRS Proc.*, 2012, **1418**, mrsf11-1418-1101-02.
- 11 S. M. Hashemnejad and S. Kundu, *Soft Matter*, 2015, **11**, 4315–4325.
- 12 M. Zabet, S. Mishra and S. Kundu, *Rsc. Adv.*, 2015, **5**, 83936–83944.
- 13 A. J. Peters and T. P. Lodge, *Macromolecules*, 2016, **49**, 7340–7349.
- 14 M. Zabet, S. Mishra, R. Boy, K. B. Walters, A. K. Naskar and S. Kundu, *J. Polym. Sci. Part B Polym. Phys.*, 2017, **55**, 877–887.
- 15 C. Y. Liaw, K. J. Henderson, W. R. Burghardt, J. Wang and K. R. Shull, *Macromolecules*, 2015, **48**, 173–183.
- 16 R. A. Mrozek, B. Leighliter, C. S. Gold, I. R. Beringer, J. H. Yu, M. R. Vanlandingham, P. Moy, M. H. Foster and J. L. Lenhart, *J. Mech. Behav. Biomed. Mater.*, 2015, **44**, 109–120.
- 17 A. Bracq, G. Haugou, R. Delille, F. Lauro, S. Roth and O. Mauzac, *J. Mech. Behav. Biomed. Mater.*, 2017, **72**, 138–147.
- 18 A. P. Sudarsan, J. Wang and V. M. Ugaz, *Anal. Chem.*, 2005, **77**, 5167–5173.
- 19 R. Shankar, A. K. Krishnan, T. K. Ghosh and R. J. Spontak, *Macromolecules*, 2008, **41**, 6100–6109.
- 20 J. Y. Chen, *Tear Resistant Gels, Composites, and Cushion Articles*, 2007, US Patent 7,222,380.
- 21 K. R. Shull, *J. Polym. Sci. Part B Polym. Phys.*, 2007, **45**, 1390–1398.
- 22 K. A. Erk and K. R. Shull, *Macromolecules*, 2011, **44**, 932–939.

- 23 T. Baumberger, C. Caroli and D. Martina, *Nat. Mater.*, 2006, **5**, 552–555.
- 24 S. Kundu and A. J. Crosby, *Soft Matter*, 2009, **5**, 3963–3968.
- 25 A. N. Gent and C. Wang, *J. Mater. Sci.*, 1991, **26**, 3392–3395.
- 26 J. A. Zimmerman, N. Sanabria-Delong, G. N. Tew and A. J. Crosby, *Soft Matter*, 2007, **3**, 763–767.
- 27 S. B. Hutchens and A. J. Crosby, *Soft Matter*, 2014, **10**, 3679–3684.
- 28 S. Mishra, T. E. Lacy and S. Kundu, *Int. J. Non. Linear. Mech.*, 2018, **98**, 23–31.
- 29 T. L. Anderson, *Fracture mechanics: Fundamentals and Applications*, CRC press, 2017.
- 30 Y. Tanaka, K. Fukao and Y. Miyamoto, *Eur. Phys. J. E*, 2000, **401**, 395–401.
- 31 T. Baumberger and O. Ronsin, *J. Chem. Phys.*, 2009, **130**, 061102.
- 32 D. Bonn, *Science*, 1998, **280**, 265–267.
- 33 N. Shahidzadeh-Bonn, P. Vié, X. Chateau, J. N. Roux and D. Bonn, *Phys. Rev. Lett.*, 2005, **95**, 3–6.
- 34 L. Vanel, S. Ciliberto, P. P. Cortet and S. Santucci, *J. Phys. D. Appl. Phys.*, 2009, **42**, 214007.
- 35 S. N. Karobi, T. L. Sun, T. Kurokawa, F. Luo, T. Nakajima, T. Nonoyama and J. P. Gong, *Macromolecules*, 2016, **49**, 5630–5636.
- 36 G. J. Lake and A. G. Thomas, *Proc. R. Soc. A Math. Phys. Eng. Sci.*, 1967, **300**, 108–119.
- 37 J. Washiyama, E. J. Kramer and C. Y. Hui, *Macromolecules*, 1993, **26**, 2928–2934.
- 38 J. Washiyama, E. J. Kramer, C. F. Creton and C. Y. Hui, *Macromolecules*, 1994, **27**, 2019–2024.
- 39 C. F. Creton and M. Ciccotti, *Reports Prog. Phys.*, 2016, **79**, 46601.
- 40 Y. Akagi, H. Sakurai, J. P. Gong, U. I. Chung and T. Sakai, *J. Chem. Phys.*, 2013, **139**, 144905.
- 41 A. Hotta, S. M. Clarke and E. M. Terentjev, *Macromolecules*, 2002, **35**, 271–277.
- 42 M. Rubinstein and R. Colby, *Polymer Physics*, OUP Oxford, 2003.
- 43 D. Mangarj, S. K. Bhatnagar and S. B. Rath, *Die Makromol. Chemie*, 1963, **67**, 75–83.
- 44 S. R. Kline, *J. Appl. Crystallogr.*, 2006, **39**, 895–900.
- 45 W. J. Wang, Z. Ye, H. Fan, B. G. Li and S. Zhu, *Polymer*, 2004, **45**, 5497–5504.
- 46 C. Lai, W. B. Russel and R. A. Register, *Macromolecules*, 2002, **35**, 841–849.
- 47 P. L. Drzal and K. R. Shull, *Macromolecules*, 2003, **36**, 2000–2008.
- 48 R. E. Bras and K. R. Shull, *Macromolecules*, 2009, **42**, 8513–8520.
- 49 H. Watanabe, T. Sato and K. Osaki, *Macromolecules*, 2000, **33**, 2545–2550.
- 50 T. L. Chantawansri, T. W. Sirk and Y. R. Sliozberg, *J. Chem. Phys.*, 2013, **138**, 1–11.
- 51 T. L. Chantawansri, T. W. Sirk, R. A. Mrozek, J. L. Lenhart, M. Kröger and Y. R. Sliozberg, *Chem. Phys. Lett.*, 2014, **612**, 157–161.
- 52 M. Rubinstein and S. P. Obukhov, *Macromolecules*, 1993, **26**, 1740–1750.
- 53 N. Mischenko, K. Reynders, M. H. J. Koch, K. Mortensen, J. S. Pedersen, F. Fontaine, R. Graulus and H. Reynaers, *Macromolecules*, 1995, **28**, 2054–2062.
- 54 R. H. Ewoldt, *J. Rheol.*, 2013, **57**, 177–195.
- 55 S. M. Hashemnejad and S. Kundu, *J. Polym. Sci. Part B Polym. Phys.*, 2016, **54**, 1767–1775.
- 56 C. Storm, J. J. Pastore, F. C. MacKintosh, T. C. Lubensky and P. A. Janmey, *Nature*, 2005, **435**, 191–194.
- 57 J. F. Douglas and J. B. Hubbard, *Macromolecules*, 1991, **24**, 3163–3177.
- 58 B. R. Chapman, M. W. Hamersky, J. M. Milhaupt, C. Kostelecky, T. P. Lodge, E. D. von Meerwall and S. D. Smith, *Macromolecules*, 1998, **31**, 4562–4573.
- 59 J. Lu, F. S. Bates and T. P. Lodge, *Macromolecules*, 2016, **49**, 1405–1413.
- 60 H. Yokoyama and E. J. Kramer, *Macromolecules*, 1998, **31**, 7871–7876.
- 61 H. Yokoyama, E. J. Kramer and G. H. Fredrickson, *Macromolecules*, 2000, **33**, 2249–2257.
- 62 L. R. G. Treloar, *The Physics of Rubber Elasticity*, Oxford University Press, USA, 1975.
- 63 S. Ravindranath and S. Q. Wang, *J. Rheol.*, 2008, **52**, 341–358.
- 64 T. F. Juliano, A. M. Forster, P. L. Drzal, T. Weerasooriya, P. Moy and M. R. Vanlandingham, *J. Mater. Res.*, 2006, **21**, 2084–2092.
- 65 T. Brenner, S. Matsukawa, K. Nishinari and R. Johannsson, *J. Nonnewton. Fluid Mech.*, 2013, **196**, 1–7.
- 66 X. Wang and W. Hong, *Soft Matter*, 2012, **8**, 8171–8178.
- 67 A. Guarino, S. Ciliberto and A. Garcimartin, *Europhys. Lett.*, 1999, **47**, 456–461.
- 68 J. Kierfeld and V. M. Vinokur, *Phys. Rev. Lett.*, 2006, **96**, 3–6.
- 69 S. Mora, *Soft Matter*, 2011, **7**, 4908–4917.
- 70 Y. Pomeau, *Comptes rendus l'Académie des Sci. Série 2, Mécanique, Phys. Chim. Sci. l'univers, Sci. la Terre*, 1992, **314**, 553–556.
- 71 M. K. Chaudhury, *J. Phys. Chem. B*, 1999, **103**, 6562–6566.
- 72 K. R. Shull, *Mater. Sci. Eng. R Reports*, 2002, **36**, 1–45.

- 73 S. Kundu and E. P. Chan, *Adhesion Behavior of Soft Materials*, Springer New York, 2012, pp. 89–125.
- 74 E. Raphaël and P. de Gennes, *Soft Order in Physical Systems*, Springer, 1994, pp. 57–71.
- 75 J. P. Gong, Y. Katsuyama, T. Kurokawa and Y. Osada, *Adv. Mater.*, 2003, **15**, 1155–1158.
- 76 T. L. Sun, T. Kurokawa, S. Kuroda, A. B. Ihsan, T. Akasaki, K. Sato, M. A. Haque, T. Nakajima and J. P. Gong, *Nat. Mater.*, 2013, **12**, 932–937.
- 77 J. van Meerveld, *Rheol. Acta*, 2004, **43**, 615–623.
- 78 L. Hong, F. Jin, J. Li, Y. Lu and C. Wu, *Macromolecules*, 2008, **41**, 8220–8224.



Failure behavior of a physically assembled gel was studied and the energy release rate was linked to the gel structure